Monthly Notices
of the
ROYAL ASTRONOMICAL SOCIETY

Mon. Not. R. Astron. Soc. **410,** 179–189 (2011) doi:10.1111/j.1365-2966.2010.17433.x

Puzzling thermonuclear burst behaviour from the transient low-mass X-ray binary IGR J17473−2721

J. Chenevez,[1⋆] D. Altamirano,[2] D. K. Galloway,[3,4] J. J. M. in 't Zand,[5] E. Kuulkers,[6] N. Degenaar,[2] M. Falanga,[7] E. Del Monte,[8] Y. Evangelista,[8] M. Feroci[8] and E. Costa[8]

[1] *National Space Institute, Technical University of Denmark, Juliane Maries Vej 30, 2100 Copenhagen, Denmark*
[2] *Astronomical Institute, 'Anton Pannekoek', University of Amsterdam, Science Park 904, 1098 XH Amsterdam, the Netherlands*
[3] *Center for Stellar and Planetary Astrophysics, Monash University, VIC 3800, Australia*
[4] *School of Physics, Monash University, VIC 3800, Australia*
[5] *SRON Netherlands Institute for Space Research, Sorbonnelaan 2, 3584 CA Utrecht, the Netherlands*
[6] *ISOC, ESA/ESAC, Urb. Villafranca del Castillo, PO Box 50727, E-28080 Madrid, Spain*
[7] *International Space Science Institute, Hallerstrasse 6, CH-3012 Bern, Switzerland*
[8] *INAF/IASF, via Fosso del Cavaliere 100, I-00133 Roma, Italy*

Accepted 2010 July 27. Received 2010 July 27; in original form 2010 May 12

ABSTRACT

We investigate the thermonuclear bursting behaviour of IGR J17473−2721, an X-ray transient that in 2008 underwent a 6-month long outburst, starting (unusually) with an X-ray burst. We detected a total of 57 thermonuclear bursts throughout the outburst with *AGILE*, *Swift*, *Rossi X-ray Timing Explorer* (*RXTE*) and the *INTErnational Gamma-Ray Astrophysics Laboratory (INTEGRAL)*. The wide range of inferred accretion rates (between <1 and ≃20 per cent of the Eddington accretion rate $\dot{m}_{\rm Edd}$) spanned during the outburst allows us to study changes in the nuclear burning processes and to identify up to seven different phases. The burst rate increased gradually with the accretion rate until it dropped (at a persistent flux corresponding to ≃15 per cent of $\dot{m}_{\rm Edd}$) a few days before the outburst peak, after which bursts were not detected for a month. As the persistent emission subsequently decreased, the bursting activity resumed at a much lower rate than during the outburst rise. This hysteresis may arise from the thermal effect of the accretion on the surface nuclear burning processes, and the time-scale is roughly consistent with that expected for the neutron star crust thermal response. On the other hand, an undetected 'superburst', occurring within a data gap near the outburst peak, could have produced a similar quenching of burst activity.

Key words: binaries: close – stars: individual: IGR J17473−2721 – stars: individual: XTE J1747−274 – stars: neutron – X-rays: binaries – X-rays: bursts.

1 INTRODUCTION

X-ray bursters are accreting neutron stars (NS) in low-mass X-ray binary (LMXB) systems, in which hydrogen (H) and helium (He) accumulate on the surface, periodically exploding in thermonuclear runaways. These thermonuclear flashes, observed as Type I X-ray bursts (e.g. Lewin, van Paradijs & Taam 1993), and hereafter simply called X-ray bursts, are caused by the high temperatures and densities reached at the base of the fuel layer. Such X-ray bursts are characterized by blackbody emission with peak temperature $kT \simeq 2$–3 keV and a light curve showing a fast rise and exponential decay (for reviews, see Lewin et al. 1993; Strohmayer & Bildsten 2006). To date, a total of 92 X-ray bursters have been identified in the Milky Way (e.g. in 't Zand et al. 2004; Liu, van Paradijs & van den Heuvel 2007).[1] Many burst sources exhibit 'photospheric radius expansion' (PRE) bursts, attributed to radiation pressure exceeding the gravitational attraction in the photosphere. Strong variations of the blackbody radius are then observed simultaneously with inverse variations of the colour temperature at a constant luminosity, roughly equal to the Eddington limit ($L_{\rm Edd}$). Such bursts may thus be used to estimate the distance to the burst sources (e.g. Basinska et al. 1984).

The unstable thermonuclear burning is a recurrent phenomenon for which ignition conditions depend primarily on the (local) mass accretion rate. Early theoretical studies (Fujimoto, Hanawa & Miyaji 1981; Fushiki & Lamb 1987) predict three distinct

⋆E-mail: jerome@space.dtu.dk

[1] http://www.sron.nl/∼jeanz/bursterlist.html

nuclear burning regimes as a function of increasing accretion rate per unit area $\dot{m}$ of H/He-rich material with solar metallicity (see also Strohmayer & Bildsten 2006): unstable H ignition triggers He flashes for $\dot{m} \lesssim 900$ g cm^{-2} s^{-1}, pure He flashes occur below a shell of H steadily burning in the hot CNO cycle for $900 \lesssim \dot{m} \lesssim 2000$ g cm^{-2} s^{-1} and mixed He/H bursts are triggered by unstable He ignition for $\dot{m} \gtrsim 2000$ g cm^{-2} s^{-1}. Still, the detailed physics of the nuclear burning are not completely understood. The above-mentioned thresholds depend on nuclear reaction rates, sedimentation and mixing processes in the burning layers, as well as anisotropy effects. Thus, some phenomenological issues still have to be solved, such as the drop in burst activity at a high accretion rate (e.g. Cornelisse et al. 2003), as well as the precise burst mechanism at low accretion rates of $\lesssim$1 per cent $\dot{m}_{\rm Edd}$.

Due to nuclear reaction waiting points related to a series of β decays during the burning of H in the rp process, H-dominated bursts burn slower than He-dominated bursts, through the fast triple-α reactions. The lengths of the rise times and exponential decays are therefore related to the relative amounts of H to He burnt during the bursts. However, bursts lasting several tens of minutes have also been recorded, which are now interpreted as the long burning of a thick pure He layer, accumulated over a long interval at a very low accretion rate and/or from an He donor (see e.g. in 't Zand et al. 2005; Cumming et al. 2006; Chenevez et al. 2007; Falanga et al. 2008). Even longer and more energetic nuclear bursts have been reported in rare occasions (see e.g. Keek & in 't Zand 2008) as superbursts that last up to several hours. They are thought to arise from carbon (C) burning in a thick layer below the surface of the NS (Cumming & Bildsten 2001; Strohmayer & Brown 2002). Although H/He burning is likely required to produce the C for these bursts, interestingly the occurrence of a superburst has the effect of 'quenching' normal bursting activity for weeks to months (Kuulkers 2004).

X-ray transients are ideal sources for studies of burst behaviour because they frequently experience a large range of accretion rates (and spectral states) in a short time frame. The X-ray transient source IGR J17473−2721 was discovered with the INTErnational Gamma-Ray Astrophysics Laboratory (*INTEGRAL*) in the Galactic Centre region during an outburst in 2005 April (Grebenev, Molkov & Sunyaev 2005). The source XTE J1747−274, detected by *Rossi X-ray Timing Explorer (RXTE)* in 2005 May (Markwardt & Swank 2005), was rapidly identified with IGR J17473−2721 by Kennea et al. (2005) using *Swift*/X-Ray Telescope (XRT). The source exhibited a second episode of activity between 2008 March and September, which began with a Type I X-ray burst on MJD 54552 (Del Monte et al. 2008a), thus identifying the source as an NS in an LMXB system [though the first bursts ever observed from this source are reported in Galloway et al. (2008), hereafter G08]. Only a few observations of thermonuclear flashes occurring before the start of an outburst have been recorded (e.g. Cornelisse, Wijnands & Homan 2007; Kuulkers, in 't Zand & Lasota 2009a).

The 2008 outburst of IGR J17473−2721 was well followed from its beginning by most of the high-energy satellite fleet operating at that time. *Swift*/XRT (Altamirano et al. 2008a) and *RXTE*/Proportional Counter Array (PCA; Markwardt et al. 2008) confirmed renewed accretion activity from IGR J17473−2721 at a position consistent with the burst detection by SuperAGILE (Del Monte et al. 2008a). Hard X-ray persistent emission was almost simultaneously detected by *INTEGRAL* (Baldovin Saavedra et al. 2008; Kuulkers et al. 2008). Later on, during the outburst episode, kilohertz quasi-periodic oscillations at frequencies up to $\simeq$900 Hz were detected by Altamirano et al. (2008b), after a spectral switch from a hard to a soft state. The same authors thus identified the source to belong to the class of atoll NS and, from the observation of two PRE bursts, estimated its distance to be in the range of 4.9–5.7 kpc. A detailed comparison of the IGR J17473−2721 outbursts in 2005 and 2008 is described by Zhang et al. (2009), and a study of some bursts observed in 2008 is presented by the same authors in Chen et al. (2010) that we discuss in Section 4.1.

In this paper, we investigate the bursting behaviour of IGR J17473−2721 during its outburst in 2008, so all calendar dates refer to that year. This study is based on all the bursts observed by instruments aboard *AGILE*, *Swift*, *RXTE* and *INTEGRAL*.

2 OBSERVATIONS AND DATA ANALYSIS

2.1 *AGILE*

The *AGILE* satellite mission (Tavani et al. 2008), launched on 2007 April 23, includes a hard X-ray (18–60 keV) monitor, SuperAGILE (see Feroci et al. 2007, 2010, for details), that consists of two pairs of 1D coded aperture imagers of $107^\circ \times 68^\circ$ field of view (full width zero response), and pointed to the same target. Two are oriented along one direction in the sky and the other two in the orthogonal direction. In the overlapping region, of $68^\circ \times 68^\circ$, both coordinates are encoded, thus giving twice a 1D imaging, and the sensitivity on axis is of the order of 15 mCrab at 5σ in 1 d.

SuperAGILE is equipped with ground trigger software (see Del Monte et al. 2008b, for details), dedicated to the detection of γ-ray and X-ray bursts, as well as other transients, occurring on timescales from 512 to 8192 ms. The trigger sensitivity in 10 s at 5σ corresponds to about 1.3 Crab, assuming a Crab-like spectrum, or to 4.8×10^{-9}erg cm^{-2}s^{-1}, assuming a 3-keV blackbody spectrum. In the case of a trigger, an image is extracted and the burst position can be reconstructed with an uncertainty of 3-arcmin radius.

2.2 *Swift*

The NASA mission *Swift* (Gehrels et al. 2004) provides 15–50 keV light curves using the Burst Alert Telescope[2] (BAT; Barthelmy et al. 2005), with which we followed the long-term hard X-ray evolution of the outburst of IGR J17473−2721.

Following the burst detection by SuperAGILE (see Section 3.2), Altamirano et al. (2008a) obtained a *Swift* observation to conclusively identify the burst source with IGR J17473−2721 on 31 March (MJD 54556). We analysed data from the XRT (0.2–10 keV; Burrows et al. 2005) in both photon counting (PC) and windowed timing (WT) modes, resulting in exposure times of 4.1 and 0.7 ks, respectively. The raw data were processed with the XRT pipeline using standard quality cuts (event grades 0–2 and 0–12 for the WT and PC modes, respectively). The PC spectrum was fitted with XSPEC. version 12 (Arnaud 1996) to a simple absorbed power-law model of index 1.85 with a reduced $\chi^2 = 1.24$ for 187 degrees of freedom.

During the portion of the observation for which WT data were available, a Type I X-ray burst was detected with a peak count rate of above 400 counts s^{-1}. We carried out time-resolved spectroscopy by extracting source events from a rectangular box of 40 pixels along the image strip and 20 pixels wide. According to Romano et al. (2006), WT data at such high count rates are expected to be affected by pile-up, so we excluded a box of the central 4×20 pixels for intervals in which the count rate exceeded 400 counts s^{-1},

[2] http://swift.gsfc.nasa.gov/docsd/swift/results/transients

2×20 pixels for rates of 300–400 counts s^{-1} and a band of 1×20 pixels for count rates between 100 and 300 counts s^{-1}. The burst-time-resolved spectral analysis was performed dividing up the burst into seven intervals from 2 to 100 s. These data were fitted using XSPEC with a blackbody model subject to interstellar absorption, fixing the hydrogen column density to the value found from fitting the PC spectral data ($N_{\rm H} = 4.39 \pm 0.35 \times 10^{22}$ cm^{-2}).

2.3 *INTEGRAL*

The hard X-ray and γ-ray observatory *INTEGRAL* (Winkler et al. 2003) provides three coded-mask instruments operating simultaneously. For our study, we used the Joint European X-ray Monitor (JEM-X) (3–25 keV; Lund et al. 2003) and Imager on Board the *INTEGRAL* Satellite/*INTEGRAL* Soft Gamma Ray Imager (IBIS/ISGRI) (18 keV–10 MeV; Lebrun et al. 2003) data, reduced with the standard Off-line Science Analysis (Courvoisier et al. 2003) software version 8.0. Data were corrected for vignetting effects of the JEM-X collimator. A systematic error of 3 per cent per channel was applied to JEM-X and ISGRI spectra, corresponding to the current estimated uncertainties in their response. Due to the partly incomplete coded-mask pattern of JEM-X, its signal deconvolution can be affected by some cross-talk between sources inside the same field of view. We have verified that the source-extracted signal for the analysis of IGR J17473−2721 burst events was not contaminated by neighbouring sources.[3]

The outburst of IGR J17473−2721 was monitored as part of *INTEGRAL* regular observations of the Galactic bulge performed each spring and fall, approximately every 3 d for about 3.5 h (Kuulkers et al. 2007). In 2008, this monitoring programme covered IGR J17473−2721 between February 11 (MJD 54507) and April 20 (MJD 54516), and again between August 18 (MJD 54696) and October 22 (MJD 54761). More *INTEGRAL* data originate from long observations of the Galactic Centre region performed on April 6 (MJD 54562). We searched for X-ray bursts by scrutinizing the light curves obtained from every pointing within $\leq 5^\circ$ (JEM-X) and $\leq 12^\circ$ (ISGRI) of the source position, for a total effective exposure of about 500 and 940 ks, respectively.

2.4 *RXTE*

We used data taken by the three instruments on board NASA's *RXTE*. The densest coverage of the outburst at 2.5–12 keV is provided by the All-Sky Monitor (ASM; Levine, Bradt & Cui 1996) publicly available light curves.

PCA (Jahoda et al. 2006) consists of five large area Proportional Counter Units (PCUs). We used data from PCU2 as it was always on during the relevant observations. The PCA data set is composed of two independent series of observations between April 4 (MJD 54560) and May 22 (MJD 54608), as well as regular public observations from May 23 (MJD 54609) to October 2 (MJD 54741). The pointing was offset by $0^\circ.25$ in order to avoid GX 3+1 falling inside the $\approx 1^\circ$ PCA field of view, and no other nearby burst sources were active during that period. The *RXTE*/PCA observations were performed about every day during the outburst, with typically $\simeq$2.6-ks non-interrupted exposure each time. The total source exposure is 490 ks.

We followed the evolution of the persistent emission during the outburst by comparing, for each PCA observation, its intensity, defined as the count rate in the 2–16 keV energy band, with its hardness, defined as the ratio of the intensity in the 9.7–16 keV band to that in the 6–9.7 keV band. We thus drew a hardness–intensity diagram (HID) where these quantities are normalized to the corresponding values obtained with the Crab (see Altamirano et al. 2008c, for a full description of the procedure). We fitted the vignetting-corrected PCU2 spectra of the 2.5–25 keV persistent emission of IGR J17473−2721 with a model consisting of a blackbody radiation plus a power-law and a Gaussian emission line at 6.4 keV (consistent with Fe I Kα fluorescence) all absorbed by interstellar matter. The High-Energy X-ray Timing Experiment (HEXTE; Rothschild et al. 1998) was used to extend the bandpass with 30–200 keV. This allowed us to acquire bolometric correction factors (see G08) on the PCU2 spectra for six distinct epochs (see also Zhang et al. 2009), in order to estimate the bolometric persistent fluxes between 0.1 and 200 keV.

We searched for and analysed the bursts detected by the PCA following G08. We computed 1-s light curves on the full PCA energy range (2–60 keV) using 'Standard-1' mode data and searched for significant deviations from the mean level. For each candidate event we identified, we computed burst spectra using (typically) 64-channel 'Event mode' data from before the burst start through to late in the burst tail (typically $\approx$200 s following the burst start). The integration time for each spectrum was 0.25 s at the start of the burst, increasing through the tail as the burst flux decreased to maintain approximately the same signal-to-noise ratio level. We used a 16-s persistent spectrum (including the instrumental background) extracted from before the burst start as background for the burst spectral analysis. We fitted each spectrum initially with an absorbed blackbody, with the neutral column density $N_{\rm H}$ free to vary, and calculated its mean value over the burst. Subsequently, we re-fitted the burst data with $N_{\rm H}$ frozen at the mean level and computed the bolometric flux and uncertainties based on the measured blackbody temperature and radius. Fluxes were eventually corrected for the off-axis pointing by scaling the measured flux with the ratio of the response of the collimator at the aim point to its response at the source position.

2.5 Burst properties

We apply the definitions by G08 for burst start and rise times, as the time when the burst flux first exceeds 25 per cent of the peak flux and the following interval until the burst exceeds 90 per cent of the peak flux, respectively. We define the burst duration as the interval from the start time to the time when the burst flux has decayed to 25 per cent of the peak flux. All uncertainties are given at a 1σ confidence level.

We compute the burst fluence $F_{\rm b}$ by integrating the measured flux over the burst duration, the burst time-scale τ as the ratio of the fluence to the peak flux and $\alpha = (F_{\rm pers}/F_{\rm b})\Delta t_{\rm rec}$ as the energy ratio of persistent emission to bursts (e.g. Lewin & Joss 1983), where $\Delta t_{\rm rec}$ is the recurrence time between two consecutive bursts, $F_{\rm pers}$ is the persistent flux at the time of the second burst and $F_{\rm b}$ is the fluence of this burst.

3 RESULTS

3.1 Persistent emission

We follow the changes of the broad-band persistent emission from IGR J17473−2721 by combining BAT daily averaged data with

[3] In particular GX 3+1, located $0^\circ.8$ away from IGR J17473−2721 and which at that time was in a high-soft, not bursting state.

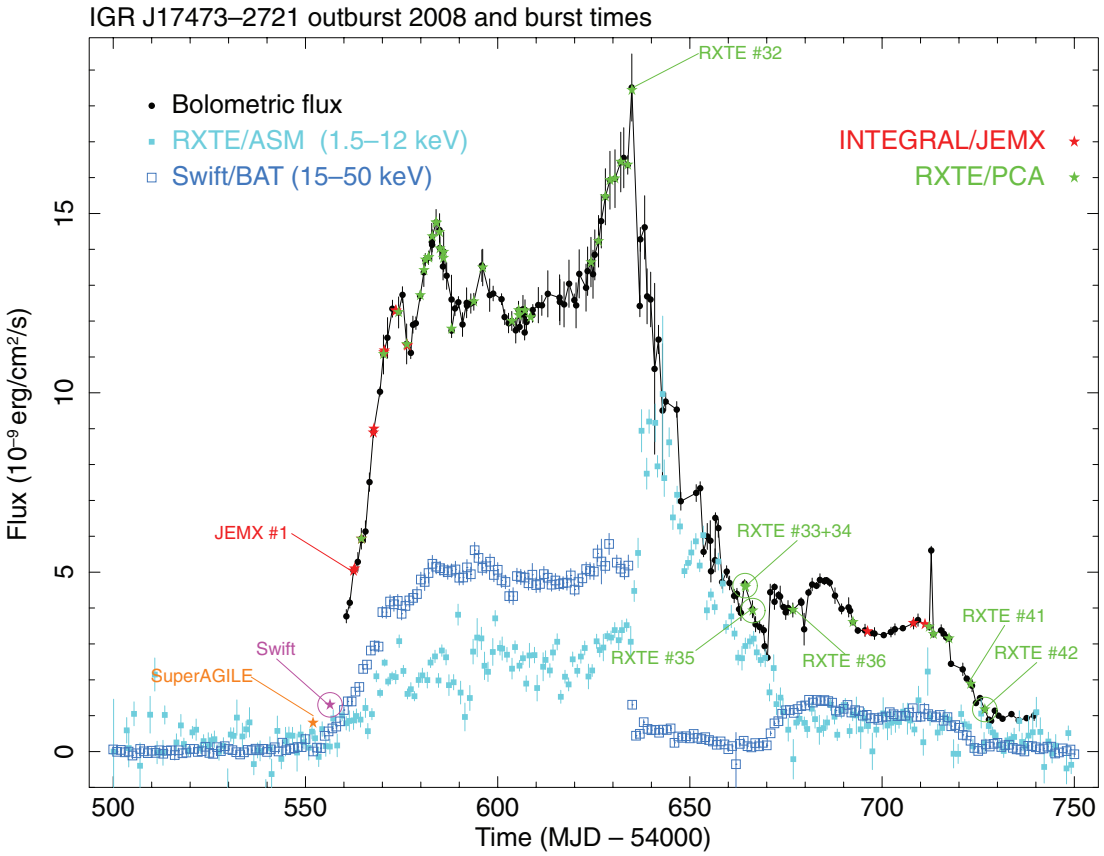

Figure 1. Broad-band X-ray light curves for IGR J17473−2721 during the 2008 outburst, combining all available *RXTE* and *Swift*/BAT 1-day averaged data. The bolometric fluxes are derived from *RXTE*/(PCA+HEXTE) fits (see the text) and have been connected for clarity. Every PCA observation is represented by a black dot. The observed X-ray bursts are represented by stars, with circles for the four PRE ones, and those indicated by names delineate the transitions between different phases of burst behaviour (see Sections 3.3 and 4.1).

all available *RXTE* data between MJDs 54500 and 54750 (MJDs 54560–54740 for PCA and HEXTE).

Fig. 1 depicts the evolution of the bolometric flux of IGR J17473−2721 together with ASM and BAT daily averaged light curves for the soft and hard persistent intensities, respectively. The outburst started at the end of March, around MJD 54556 (see also Kuulkers et al. 2008; Markwardt et al. 2008; Altamirano et al. 2008a), with a rapid rise in intensity, particularly in hard (>15 keV) X-rays, and reached a bolometric flux of $\simeq 1.3 \times 10^{-8}$ erg cm^{-2} s^{-1} in less than 20 d. The source remained close to this flux level during the following one and a half month (from around MJD 54580 to 54625). The flux then rose for another 10 d, reaching a peak of about 18.5×10^{-9} erg cm^{-2} s^{-1} on June 17 (MJD 54634). At the same time, the persistent spectrum dramatically switched from hard (i.e. with more flux in the 15–50 keV band than in the <12-keV band) to soft in less than 3 d, as witnessed by ASM and BAT light curves (Fig. 1). These two states are also obvious in the HID plotted in Fig. 2 that shows the transition with the 9.7–16/6–9.7 keV hardness falling abruptly from above 1 down to below 0.6 at a 2–16 keV flux slightly increasing above 0.2 Crab. The bolometric flux subsequently decreased almost continuously for about 1 month (from MJD 54635 to 54670), down to $\simeq 3 \times 10^{-9}$ erg cm^{-2} s^{-1}. From MJD 54670.5 the source spectral state returned from soft to hard at a relatively low level (corresponding to the group near the middle of the HID at the hardness around 1), remaining there for a month at a bolometric flux level of about 4×10^{-9} erg cm^{-2} s^{-1} and finally

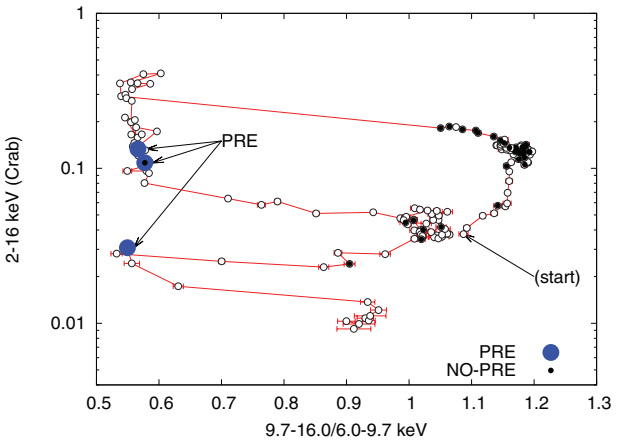

Figure 2. X-ray HID obtained from *RXTE*/PCA data for IGR J17473−2721 during its outburst in 2008. Hardness and intensity are normalized to the Crab. The positions of the X-ray bursts observed by *RXTE* are shown through filled circles (large for PRE bursts). The arrow indicates the first measurement at MJD 54560.

decreased, with a hardness zigzag path, back to its pre-outburst level after another month (see also Zhang et al. 2009).

We note that the HID shows some similarities with the corresponding diagrams for black-hole X-ray binaries (see e.g. Fender, Belloni & Gallo 2004), and similarities in this sense have already

been reported (e.g. Fender & Kuulkers 2001; Fender, Gallo & Jonker 2003; Tudose et al. 2009).

3.2 Burst analysis

We found a total of 57 individual X-ray bursts from IGR J17473−2721 in 2008. One of these bursts, on April 8 (MJD 54564.567), was simultaneously detected by *INTEGRAL*/JEM-X and *RXTE*/PCA. We have performed separate light curve and spectral analyses of each burst data set from the different instruments: SuperAGILE: one burst, XRT: one burst, JEM-X: 14 bursts (of which six were also weakly detected by ISGRI) and PCA: 42 bursts.

3.2.1 Burst light curves

The first X-ray burst from IGR J17473−2721 in 2008 was detected by SuperAGILE on March 26 (MJD 54551.972) at a time when the source was in relative quiescence at a 2–10 keV flux below $\simeq 10^{-10}$ erg cm^{-2} s^{-1} (Kuulkers et al. 2008; Markwardt et al. 2008; Del Monte et al. 2008a). The event was visible only in the SuperAGILE 17–25 keV band light curve (see Fig. A1) for a duration of 44 s. The broad single peak, showing some hints of internal structure, was not preceded by a precursor. From the SuperAGILE image in the same energy band, the average flux is derived to $\simeq 3.1 \pm 0.6 \times 10^{-9}$ erg cm^{-2} s^{-1} and the burst fluence is $\simeq 1.4 \pm 0.3 \times 10^{-7}$ erg cm^{-2}. The hardness ratio (counts between 20 and 25 keV divided by the counts between 17 and 20 keV) does not show any evolution during the burst. We did not find other bursts from the same source in SuperAGILE data during the whole *AGILE* observation from 20.7 d prior to 3.5 d after the burst.

A few days later, on March 31 (MJD 54556.377), the XRT and BAT instruments detected a second X-ray burst (see Fig. 3) when the 2–10 keV source persistent flux was still low at $\simeq 3 \times 10^{-10}$ erg cm^{-2} s^{-1} (Altamirano et al. 2008a). The 2–10 keV burst rise time is 4.5 s and the bolometric peak flux is $1.09 \pm 0.08 \times 10^{-7}$ erg cm^{-2} s^{-1}. The decay consists of a first prompt decrease with an e-folding decay time of 12 s, followed 14 s after the burst peak by a longer tail decreasing with an e-folding decay time of 25 s; the single exponential decay time for the whole light curve is 21 s. The 17–25 keV BAT light curve (see Fig. 3) allows us to compare this burst with the SuperAGILE one in the same energy band and indicates a burst duration of $\simeq$20 s, about a factor of 2 shorter than the burst observed by SuperAGILE. In this energy band, the average BAT burst flux is $\simeq 3.8 \pm 1.5 \times 10^{-9}$ erg cm^{-2} s^{-1} and the fluence is about $0.7 \pm 0.1 \times 10^{-7}$ erg cm^{-2}. Moreover, we note that the hard X-ray light curve shows a double-peaked structure, which is often related to a PRE event (see Section 3.2.2).

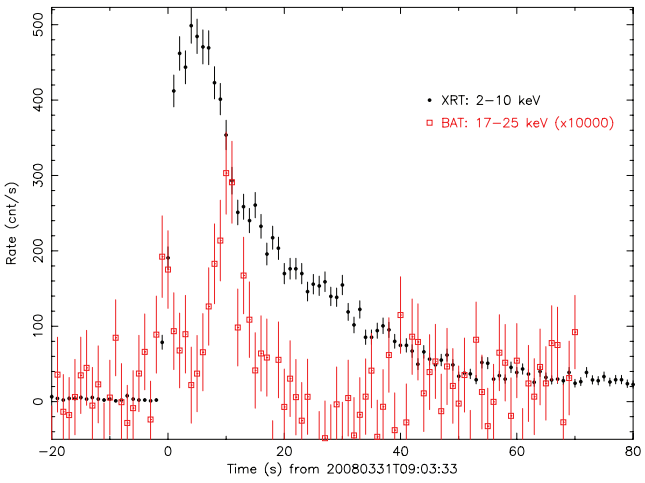

Figure 3. 1-s bin light curves of the X-ray burst observed by *Swift* on March 31 (MJD 54556.377).

INTEGRAL detected 14 X-ray bursts near the beginning and the end of the outburst of IGR J17473−2721 (see Fig. A2 and Table A1). Thanks to the long uninterrupted *INTEGRAL* observations on the source, we recorded five pairs of bursts from which we can unambiguously measure the wait times between the bursts, which decreased from 6.5 h on MJD 54562 down to 2.1 h on MJD 54576. The first 11 bursts, observed during the outburst rise, have relatively long rise times of between 3 and 9 s (5.2 ± 1.8 s on average) and long exponential decay times of between 10 and 33 s (14.5 ± 4.5 s on average). The three remaining bursts, observed during the outburst tail, evolved more rapidly, with rise times of between 1 and 5 s (average $= 2.7 \pm 1.0$ s) and decays of between 9 and 14 s (average $= 10.3 \pm 1.4$ s). Among the bursts also detected by the IBIS/ISGRI instrument, two were significant up to 40 keV. As a comparison with the first two bursts observed by SuperAGILE and *Swift*, the 17−25 keV light curve of the first burst observed by *INTEGRAL* on April 6 (MJD 54562.508) indicates a duration of only $\simeq$8 s.

The richest data set is provided by PCA, covering most of the outburst. The bolometric flux light curves of the 42 bursts detected by PCA have been compiled in Fig. 4 (see also Table A1). Burst 1 is the event simultaneously detected by JEM-X on MJD 54564.567, though their light curves are not easy to compare because the JEM-X and PCA instruments have different responses. Bursts 8 and 9 form a doublet only separated by 510 s. Observations of a few burst pairs indicate a steadily decreasing wait time to a minimum of 1.6 h at MJD 54585. We notice a prolonged pause of burst activity after the outburst emission reached its bolometric peak flux, also corresponding to the sudden change in spectral hardness (Figs 1 and 2). The last recorded burst before the peak of the outburst is 32, and the next recorded burst, 33, was observed 1 month later. The difference between the light curves of these two bursts is clear and indicates a major change in the general shape of the burst light curves before and after the outburst peak. Thanks to the good time resolution of the PCA, the light curves can be fitted with dual exponential decays. On average, the 32 PCA bursts that occurred before the peak of the outburst have rise times of 6.6 ± 1.1 s and exponential decays of 9.7 ± 2.7 and 26.8 ± 7.4 s. The 10 remaining bursts after the resumption of the burst activity during the decay of the outburst are characterized by much shorter rise times of 4 ± 1 s on average and exponential decay times of 5.2 ± 1.6 and 14.5 ± 4.2 s on average. This is consistent with the bursts reported by JEM-X at corresponding epochs. Among the PCA bursts, 33, which is the first burst observed after the 1-month intermission, has the highest peak flux at $F_{\rm p} = 9.6 \pm 0.2 \times 10^{-8}$ erg cm^{-2} s^{-1} as well as the shortest rise time of 2.25 ± 0.25 s and shortest exponential decay time of 4.8 ± 0.5 s.

3.2.2 X-ray burst spectral analysis

We present results of time-resolved spectral analyses performed for the bursts observed with *Swift* (see Fig. 5) and *RXTE*/PCA (see Figs A3 and A4).

The time-resolved spectroscopy of the *Swift* burst reveals anti-correlated blackbody temperature and radius variations at roughly constant bolometric flux during the first 20 s. The PCA bursts 33, 35 and 42 exhibit the same properties, characteristic of PRE

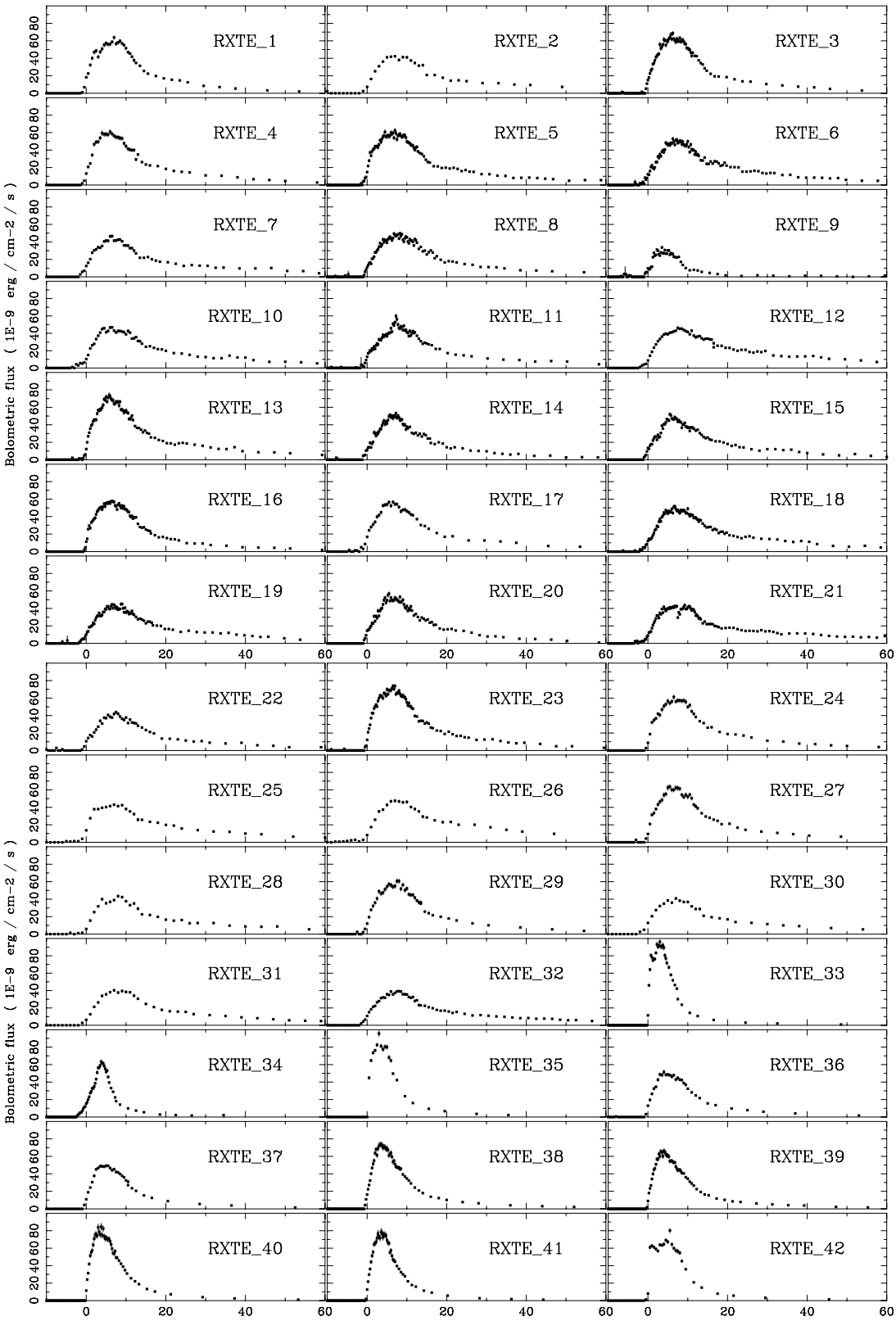

Figure 4. Chronologically ordered bolometric flux light curves of the X-ray bursts observed by *RXTE*/PCA.

events. The average bolometric peak flux of these four bursts is $F_{\rm peak} = (95 \pm 9) \times 10^{-9}$ erg cm^{-2} s^{-1} and the highest peak flux is reached by the *Swift* burst at $F_{\rm peak} = (109 \pm 9) \times 10^{-9}$ erg cm^{-2} s^{-1}. Assuming that the highest peak flux corresponds to the Eddington luminosity limit for helium bursts, $L_{\rm Edd} = 3.8 \times 10^{38}$ erg s^{-1}, as empirically derived by Kuulkers et al. 2003 (but see also Section 4.1), we derive a source distance of 5.4 ± 0.2 kpc (see also Altamirano et al. 2008a,b). In Figs 5 and A4, the blackbody radius is presented

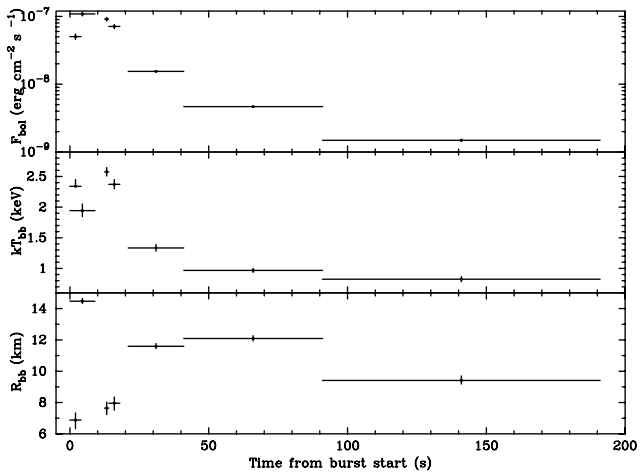

Figure 5. Time-resolved spectroscopy results of the X-ray burst observed with *Swift* on March 31 (MJD 54556.377). The blackbody radius is calculated from the fit normalization for a distance of 5.5 kpc (see Section 4.1).

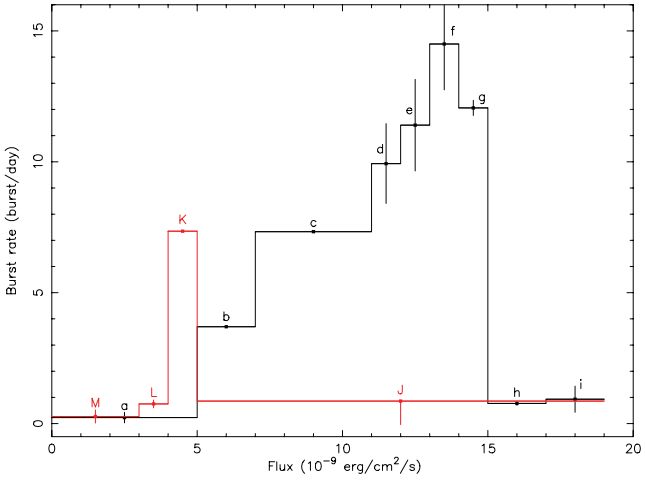

Figure 6. Plot of the IGR J17473−2721 burst rate as a function of persistent bolometric flux derived from the waiting times between two observed consecutive bursts. Bins in black (lower case letters) and red (upper case letters) correspond to pre- and post-outburst peaks, respectively. The letters indicate the number of bursts (n) and exposure times (exp in ks) per bin as follows: n/exp – a: 2/11.2, b: 3/39.8, c: 2/18.9, d: 8/50.6, e: 9/77.2, f: 8/44.1, g: 6/24.9, h: 5/16.8, i: 1/3.4, J: 0/60.2, K: 2/72.8, L: 9/55.1 and M: 2/40.9. The heights of the bins without error bars are given by one pair of bursts detected during an uninterrupted observation. The error bars are obtained either by the difference between the waiting times of two distinct pairs of bursts observed inside the same flux interval or by the difference between the averaged time from burst to burst and the shortest time within two consecutive burst detections in separated observations.

at a distance of 5.5 kpc (see Section 4.1). It is worth noting that all these PRE flashes occurred at times when the 15–50 keV intensity measured by the BAT was at its lowest level (see Fig. 1) during the soft spectral state. This can also be seen in the HID of the outburst (Fig. 2), placing the PRE bursts in the softest states.

We further note that bursts 38–41, whose temperatures peak above 3 keV, show slightly anticorrelated variations of the blackbody radius with the colour temperature, in the opposite way as PRE events. All these bursts have also in common to occur at a low persistent bolometric flux of $<3.5 \times 10^{-9}$ erg cm^{-2} s^{-1}.

Time-resolved spectral analysis results of the bursts observed by the other instruments do not provide additional information. The complete analysis results for every burst are compiled in Table A1.

3.3 Burst behaviour as a function of the bolometric flux

During the rise phase of the outburst bolometric flux, the burst recurrence time became progressively shorter, down to less than 2 h, as derived from uninterrupted observations of the source between pairs of consecutive bursts. The light curves of the bursts observed in that phase of the outburst showed slow rise and relatively long decay times (Figs 4 and A2). After the persistent flux reached its maximum, corresponding to $\simeq$15–20 per cent of the Eddington limit (see Fig. 1), no bursts were detected during a prolonged period of low flux in a soft spectral state. The burst activity resumed after an interruption of 1 month, with shorter and more intense bursts than before the peak of the outburst. Fig. A5 shows a likely correlation (Pearson's coefficient $r = 0.62$) between increasing exponential decay times and increasing persistent flux. On the other hand, we also note that the bursts with the highest peak fluxes tend to have the shortest decay times (see Fig. A6).

Apart from the PRE bursts only occurring in the soft state as already mentioned, we also notice in the HID (Fig. 2) that there are more bursts in the hard state than in the soft state, all above a 2–16 keV intensity of 0.25 Crab. The bursting activity thus also seems related to the source spectral state.

We adopt here the bolometric (0.1–200 keV) flux as a tracer of the accretion rate, but acknowledge that there may be uncertainties of the order of 40 per cent due to undetected soft components (see Thompson et al. 2008), and several per cents due to jet activity, though it is not yet clear how much it can be (Russell et al. 2010). The burst rate as a function of persistent emission (or accretion rate) plotted in Fig. 6 indicates a steady increase until a maximum of 14.5 bursts per day is reached at a bolometric flux of $\approx$13.5 $\times$ 10^{-9} erg cm^{-2} s^{-1} (the short doublet is not included in Fig. 6). The bursting activity drops rapidly above a bolometric persistent flux of $\simeq$15 $\times$ 10^{-9} erg cm^{-2} s^{-1}, corresponding to $\simeq$15 per cent of the Eddington accretion rate (see Section 3.2.2). The red histogram (labelled with uppercase letters) of Fig. 6 displays the burst rate during the decrease of the persistent emission. Indeed, no bursts were detected at all in the 30 d following the bolometric peak flux of the outburst, even though observations totalling approximately 80 ks were made with *RXTE*. Before the burst interruption, JEM-X and PCA detected 42 bursts in a total of about 280-ks exposure time, corresponding to an average burst rate of almost 13 bursts per day. Assuming the same burst rate, and that Poisson statistics describe the number of bursts observed in any given observation, the probability of detecting no bursts during the interruption is 6.1 $\times$ 10^{-6}. Even at a burst rate four times lower, this probability remains below 5 per cent. 28 *RXTE* observations, of 4.2-ks mean duration (with a standard deviation of 2.9 ks), were performed randomly during 1 month and separated on average by 1 d (15-h standard deviation). Therefore, we conclude the chance probability of having missed every burst in that period to be negligible. In other words, the burst rate must have dropped considerably below an upper limit that, from the available observations, we assess at $\simeq$0.86 burst per day (at 1σ), which corresponds to the label 'J' in Fig. 6. The burst activity thus resumed ('K') about 1 month after the outburst peak and decreased later on with the decreasing persistent emission ('L' and 'M'). So, for the same range of bolometric fluxes, the bursting activity in IGR J17473−2721 strongly depends on whether

the persistent emission is increasing or decreasing. Moreover, we note from Figs A5 and 6 that, apart from the two bursts observed by SuperAGILE and *Swift* at the beginning of the outburst, the bursts observed during the rise phase of the outburst occurred at a persistent bolometric flux above 5×10^{-9} erg cm^{-2} s^{-1}, while all the bursts observed during the outburst decrease phase occurred below this threshold.

4 DISCUSSION

4.1 Summary of main results

Thanks to the wide coverage by *RXTE*, *INTEGRAL*, *Swift* and *AGILE* and their 58 burst detections, the 6-month long outburst from the transient IGR J17473−2721 provides a comprehensive record of burst activity on an NS over a wide range of accretion rates. The most interesting aspect of this record is the hysteresis shown in Fig. 6, particularly the 1-month long intermission in burst activity that commences with the peak of the accretion outburst and at the same time of a spectral state change in the accretion radiation. Similar burst intermissions also seem to have been exhibited by the bursting transients EXO 1745−248 (G08) and 4U 1608−52 (Keek et al. 2008).

From the observation of PRE bursts, we derive the distance to the source at $\simeq$5.4 kpc by assuming the highest burst peak flux equal to the Eddington limit for an H-poor photosphere: $L_{\rm Edd} = 3.8 \times 10^{38}$ erg s^{-1} (Kuulkers et al. 2003). It is, however, not possible a priori to know exactly the composition of the NS photosphere. The accreted material is most likely H-rich, based on the α values (see below), but the NS photosphere during radius expansion may be H-poor once the outermost, H-rich layers are ejected. Such a scenario is suggested from the observations of bimodal radius-expansion burst peak fluxes in 4U 1636−536 (Sugimoto, Ebisuzaki & Hanawa 1984; Galloway et al. 2006), although the details of this mechanism remain uncertain. Though the peak fluxes of the four PRE bursts are not exactly the same, we assume that they all intrinsically reach the same Eddington luminosity (see Galloway et al. 2003, 2006). Their characteristics (fast rise and short decay) being consistent with the burning of H-poor material, we interpret their peak flux as actually reaching the Eddington limit for He and the source distance thus derived being between 5.4 and 6.3 kpc. If one assumes the theoretical value of $L_{\rm Edd} \simeq 2.9 \times 10^{38}$ erg s^{-1} for He bursts on a canonical 1.4-M$_\odot$, and 10-km radius NS (see e.g. Galloway & Cumming 2006), the distance is reduced to between 4.7 and 5.5 kpc. In conclusion, we find the distance to IGR J17473−2721 at $d = 5.5 \pm 0.8$ kpc.

A rare observation of an X-ray burst prior to the beginning of the outburst (Del Monte et al. 2008a) is the signature of some accretion activity at a particularly low rate (Kuulkers et al. 2009a). We estimate the 17–25 keV fluence of the SuperAGILE burst to about 1.4×10^{-7} erg cm^{-2}, which is twice higher than the *Swift* burst fluence in the same energy band. For a 3-keV blackbody model, this leads to a bolometric fluence of about 10^{-6} erg cm^{-2}, which is similar to the fluence of the confirmed PRE bursts observed later in the outburst. This fluence implies that accretion started at least 3 d prior to the burst observed by SuperAGILE or a week before the onset of the outburst. Alternatively, it means that some fuel was left over from the previous outburst in 2005.

We found a burst doublet with less than 10-min recurrence time. While the first of these two bursts shows relatively long rise (6.5 ± 0.3 s) and decay (>10 s) times, the second one has much shorter rise (3.5 ± 0.3 s) and decay (5 ± 0.5 s) times. The fluence of this latter burst, equal to 3.49×10^{-7} erg cm^{-2}, is three to four times lower than the previous and the other neighbour bursts. Moreover, assuming complete and isotropic burning of the fuel accreted between these two bursts, the ignition column for the second one is $y = F_{\rm pers} \times (d/R)^2 \times (1+z)/(z\,c^2) \times \Delta t \approx 10^7$ g cm^{-2}. This small ignition column, about one order of magnitude lower than for typical bursts, is insufficient to ignite freshly accreted nuclear fuel. It may therefore indicate that the second burst is related to the first one and produced by some residue of unburnt fuel as suggested by Fujimoto et al. (1987). However, other examples of burst doublets have already been observed from other sources with even shorter intervals (see e.g. G08; Linares et al. 2009), and their explanation may be related to the mixing of the unburnt fuel in deeper layers (Boirin et al. 2007; Keek et al. 2010).

One convenient way to investigate the burst energetics is to compare the amount of energy radiated by the persistent emission between the bursts with the energy released by the thermonuclear bursts. Their ratio is the α parameter, determined observationally as the ratio of the integrated persistent (bolometric) flux over the burst interval to the burst fluence (see Section 2.5). Assuming that all the accreted fuel is burnt during the bursts, the nuclear energy release per nucleon (see e.g. Galloway & Cumming 2006) is $Q_{\rm nuc} = z\,c^2/\alpha\,(10^{18}\,{\rm erg\,g})^{-1}$, where $z = 0.31$ is the appropriate gravitational redshift at the surface of a 1.4-M$_\odot$ and 10-km radius NS. For a given average mass fraction X of H at ignition, one has $Q_{\rm nuc} = 1.6 + 4X$ MeV nucleon^{-1}. During the plateau prior to the peak of the outburst of IGR J17473−2721, α is about 75–80, increasing to $\alpha \gtrsim 110$ when the bursting activity resumes after the peak of the outburst. These values correspond to H fractions in the burst fuel of $X \approx 0.50$ and $X < 0.23$, respectively. This difference in fuel composition, and thus in burning regime, may explain why the burst rate shown in Fig. 6 is higher after the outburst peak than compared to when it was at the same flux level at the beginning of the outburst.

Eventually, the originality with IGR J17473−2721 is that seven phases of burst behaviour can be distinguished in Figs 1 and 4. They are as follows.

(i) Very early in the outburst, a first burst detected with SuperAGILE, followed a few days later by the *Swift* observation of a PRE burst. Both bursts occur at a low accretion rate of $\lesssim$1 per cent of the Eddington limit.

(ii) During the rise of the outburst and the subsequent plateau phase in the hard state (from the first JEM-X burst to *RXTE* 24), bursts arrive faster with increasing accretion rates. The slope of the linear rise in the burst rate versus persistent flux histogram (Fig. 6) is equivalent to $\alpha = 80 \pm 16$, which is consistent with the direct (burst-to-burst) measurements in Table A1. Together with this value, the relatively long burst rises and decays point to He-ignited H/He bursts in which the H is burnt through the rp process (compare with burst profiles of GS 1826−24; Heger et al. 2007).

(iii) During the final $\simeq$15 d leading to the outburst peak (*RXTE* bursts 25–32), when the bolometric flux is in excess of 15×10^{-9} erg s^{-1} cm^{-2}, the recurrence time drops by an order of magnitude (Fig. 6). This leads to an increase of alpha to about 1500, consistent with simultaneous stable and unstable He burning (in 't Zand et al. 2003).

(iv) At the time of the outburst peak, a 1-month intermission in burst activity starts. The outburst peak also coincides with a sharp spectral transition into a soft state.

(v) After the intermission, when the outburst is still in the soft state, but when the persistent flux is at similar levels as during the first few bursts early in the outburst, the brightest and shortest X-ray bursts occur (*RXTE* bursts 33–35, two with PRE). Most likely, these are pure He flashes.

(vi) After the persistent spectrum switches back to a hard state within 10 d, the X-ray bursts become longer again, but not as long as earlier in the outburst, and are probably again due to mixed He/H burning (JEM-X bursts 11–14 and *RXTE* bursts 36–41).

(vii) The last observed burst (*RXTE* 42) occurs after yet another transition of the accretion radiation from a hard to a soft state at a low accretion rate. This burst also shows limited PRE.

A study of the burst activity in IGR J17473−2721 was recently published in Chen et al. (2010). As a main result, these authors find two parallel evolution groups of the burst durations as a function of the persistent luminosity. However, we note that they only employed 16 bursts during the outburst of IGR J17473−2721 in 2008, all after MJD 54624, against 57 in our data set, which spans the whole outburst. We mean that the findings of Chen et al. (2010) derive from a selection effect, for no such parallel groups are visible in Fig. A5, which corresponds to fig. 5 of Chen et al. (2010). Moreover, we note a discrepancy between our bolometric fluxes and those of Chen et al. (2010), which is most probably due to the limited energy range (1.5–30 keV) these authors adopt to define the bolometric luminosity based only on PCA measurements. Such a limited bolometric range does not adequately represent the persistent luminosity of IGR J17473−2721 and hence its mass accretion rate during the different phases of the outburst. Therefore, we do not come to the same conclusions as Chen et al. (2010) but rather suggest the following interpretations of our observation results.

4.2 Possible interpretations

There is considerable variability in burst peak fluxes and time-scales. The rise and decay times tend to be somewhat longer before the intermission than after particularly the rise times. The shortest rise times combine with the highest peak fluxes. These trends indicate a varying He to H abundance ratio in the burning layer. This is not unexpected considering the varying accretion rate. The shortest bursts (*RXTE* bursts 33–35) are consistent with pure He burning. All other bursts are longer and fainter and must have larger H fractions in the fuel. Therefore, the mass donor must be H-rich. The fact that pure He bursts occur implies that stable H burning (through the hot CNO cycle) must simultaneously be present during *RXTE* bursts 33–35, particularly since bursts at similar persistent fluxes early in the outburst (for instance, *RXTE* burst 1) have roughly twice longer time-scales and half the peak flux. Thus, we identify four burst regimes as follows: first, mixed H/He flashes during burst phases (i), (ii), (iii) and (vi); secondly, pure He flashes concurrent with stable H burning in burst phase (v); thirdly, rich He flashes at the lowest persistent fluxes; and Finally, no bursts at all and therefore stable H and He burning during the intermission. Thus, all burst regimes for H/He burning (Fujimoto et al. 1981; Bildsten 1998) are exhibited by IGR J17473−2721 but at accretion rates about 1-mag order higher. Such a discrepancy between observed and theoretical accretion rates has already been noted for other sources (see e.g. the discussion by Cornelisse et al. 2003).

The most intriguing question is what actually caused the 1-month interruption of burst activity *after* the peak of the outburst. If the He and H are not burnt in an unstable fashion through flashes, they must be burnt in a stable fashion. The drop in burst rate (Fig. 6) just before the peak thus suggests the onset of stable H and He burning, at a threshold persistent luminosity that is similar (i.e. within a factor of 2) to what is seen in other bursters (cf. Cornelisse et al. 2003), although the burst profiles in IGR J17473−2721 do not show as strong a change. Hence, stable He burning, which should occur at higher accretion rates than stable H burning, apparently starts for IGR J17473−2721 at lower accretion rates than normally expected. We discuss two scenarios.

One possibility is that the intermission is the result of thermal relaxation of the crust. The crust becomes hotter during the outburst due to electron capture reactions (Gupta et al. 2007). The thermal time-scale of the crust is of the order of a few months (Brown & Cumming 2009). It is likely that the temperature is still rising after the outburst peak. Above certain temperatures, the H and He burning will become stable (7×10^7 and 4×10^8 K, respectively; e.g. Cumming & Macbeth 2004). The intermission of bursts at the time of the peak of the outburst may be explained if the temperature rises above the threshold temperature for stable He burning just at that time. The thermal relaxation of the crust may sustain that temperature for the duration of the intermission after which it would drop below the threshold due to the decay in the accretion rate that started at the peak of the outburst. Calculations for the transient 4U 1608−52, which had a similar outburst duration and peak accretion rate to IGR J17473−2721, indicate that the temperature may reach high enough values (Keek et al. 2008). A problem of this scenario is that the heating time-scale appears short if the burning depth is the same for stable H and stable He burning. Indeed, it takes for IGR J17473−2721 less than 15 d from the onset of stable H burning (drop of burst rate) to reach stable-only He burning (burst interruption), corresponding to a difference factor of 5–6 in temperature. The rapidity of this heating may be explained by the onset of stable H burning, but verifying this requires solving the heat balance of the upper layers. As with the calculation of the thermal relaxation of the crust, this is outside the scope of this observational paper.

An alternative and perhaps more likely explanation for the intermission is that a superburst occurred during a data gap and provided the sudden heating to initiate stable He burning. There is a data gap of more than 10 h between the last detected burst and the first available observation (by *RXTE*/ASM) of the soft state. Though the probability that a superburst just occurred during the data gap is rather small – ∼0.1 per cent for a typical superburst recurrence time of ∼1 per year (Keek & in 't Zand 2008) – this is, in principle, enough time for a superburst to ignite and cool off. Cessation of burst activity after a superburst is commonly observed (e.g. Kuulkers 2004). This 'quenching' of normal bursts is explained by the additional heat flux coming from the underlying cooling ashes of the superburst that stabilizes the H/He burning layers (Cumming & Bildsten 2001). Cumming & Macbeth (2004) predict time-scales for quenching of weeks. In the cases of Ser X-1 (Cornelisse et al. 2002) and KS 731−260 (Kuulkers et al. 2002), no bursts were detected after a superburst during a period of about 1 month. Another example, more similar to the present case, is a superburst from the transient and H-rich burster 4U 1608−52 (Keek et al. 2008), 55 d after the onset of an outburst in 2005. The first normal burst was detected 100 d after the superburst, although long data gaps may have prevented earlier burst detections. Considering that the sudden burst intermission of IGR J17473−2721 began after the outburst peak at MJD 54635, a superburst would thus possibly have taken place more than 75 d after the outburst onset. The fluence of the outburst until the peak is 0.08 erg cm^{-2}, which at the distance to the source translates to an energy of 3×10^{44} erg. This is similar

to the value reported by Keek et al. (2008) before the superburst of 4U 1608−522. The average bolometric flux of the outburst prior to the maximum is 12.3×10^{-9} erg cm^{-2} s^{-1} or about 12 per cent of the Eddington limit, which corresponds to the level of accretion rate typically measured for superbursts (see e.g. Keek & in 't Zand 2008). For $\Delta t = 75$ d, this corresponds to an accumulated column depth $y = m\Delta t/(1+z) = 1.1 \times 10^{11}$ g cm^{-2}. This is one order of magnitude below the typical column depth for superbursts whose energy release is 10^{42} erg, but a part of the necessary C fuel may have been accumulated on a much longer time-scale at a low accretion rate. Still, this value is only half the value inferred from the superburst light curve of 4U 0614+091 (see Kuulkers et al. 2009b), and as discussed by these authors, such a shallow column depth would require for ignition that the temperature of the NS crust is above 6×10^8 K. As previously mentioned, both stable and unstable He burning likely occurred during the 15 d prior to the outburst peak of IGR J17473−2721, thus increasing considerably the C production. It is also worth noting that Cornelisse et al. (2002) find that the low-energy flux increased significantly after the superburst of Ser X-1 as well as after the superburst from 4U 1735−44 (Cornelisse et al. 2000), like in IGR J17473−2721.

Burst regimes appear to be tightly connected to positions in the HID (see Fig. 2). The last five phases of burst behaviour (see above) correspond to five distinct regions in the HID. A straightforward explanation is that both have a common driver: the accretion rate. Changes of burst regimes could be connected to threshold values in the (local) accretion rate and likewise could changes in spectral states of the persistent radiation be. What is remarkable for IGR J17473−2721 is that one change in burst regime occurs at the same time and/or at the same accretion rate as one change in the spectral state, and this is more clear than for other sources (see also G08). If one refuses this as a coincidence, one could change the logic: the spectral state change may be due to the missed superburst or the onset of a stable He fusion process. Again, it is interesting to compare with 4U 1608−52, for which Yu & van der Klis (2002) suggest that nuclear burning on the NS surface leads to the radiative truncation of the inner accretion disc.

In conclusion, the burst properties of IGR J17473−2721 are consistent with an NS accreting H-rich material at varying rates all along the outburst episode. The bursting rate as a function of the accretion rate displays a hysteresis on either side of the peak of the outburst, coincident with the interruption of the burst activity. This hysteresis may be explained by the thermal response of the NS crust or the occurrence of a superburst. Though the odds of having missed a superburst inside a data gap of only 10 h are not high, we consider that explanation as more likely than thermal relaxation of the crust. The question is whether the occurrence of this undetected superburst is related to the abrupt spectral transition the source underwent short after the peak of the outburst.

ACKNOWLEDGMENTS

We are grateful to Andrew Cumming and Rudy Wijnands for fruitful discussions. JC acknowledges financial support from the Instrument Centre for Danish Astronomy and ESA/PRODEX Nr. 90057. *Swift*/BAT transient monitor results are provided by the *Swift*/BAT team and *RXTE*/ASM results are provided by ASM/*RXTE* teams at MIT and at the *RXTE* SOF and GOF at NASA's GSFC. This work is partly based on observations with *INTEGRAL*, an ESA project with instruments and science data centre funded by ESA member states (especially the PI countries: Denmark, France, Germany, Italy, Switzerland and Spain), Czech Republic and Poland, and with the participation of Russia and the USA.

REFERENCES

Altamirano D., Degenaar N., in 't Zand J., Markwardt C., Wijnands R., 2008a, Astron. Tel., 1459
Altamirano D. et al., 2008b, Astron. Tel., 1651
Altamirano D., van der Klis M., Méndez M., Jonker P. G., Klein-Wolt M., Lewin W. H. G., 2008c, ApJ, 685, 436
Arnaud K. A., 1996, in Jacoby G. H., Barnes J., eds, ASP Conf. Ser. Vol. 101, Astronomical Data Analysis Software and Systems V. Astron. Soc. Pac., San Francisco, p. 17
Baldovin Saavedra C. et al., 2008, Astron. Tel., 1468
Barthelmy S. D. et al., 2005, Space Sci. Rev., 120, 143
Basinska E. M., Lewin W. H. G., Sztajno M., Cominsky L. R., Marshall F. J., 1984, ApJ, 281, 337
Bildsten L., 1998, in Buccheri R., van Paradjis J., Alpar M. A., eds, The Many Faces of Neutron Stars. Kluwer, Dordrecht, p. 419
Boirin L., Keek L., Méndez M., Cumming A., in 't Zand J. J. M., Cottam J., Paerels F., Lewin W. H. G., 2007, A&A, 465, 559
Brown E. F., Cumming A., 2009, ApJ, 698, 1020
Burrows D. N. et al., 2005, Space Sci. Rev., 120, 165
Chen Y., Zhang S., Torres D. F., Wang J.-M., Li T.-P., 2010, A&A, 510, 81
Chenevez J. et al., 2007, A&A, 469, L27
Cornelisse R., Heise J., Kuulkers E., Verbunt F., in 't Zand J. J. M., 2000, A&A, 357, L21
Cornelisse R., Kuulkers E., in 't Zand J. J. M., Verbunt F., Heise J., 2002, A&A, 382, 174
Cornelisse R. et al., 2003, A&A, 405, 1033
Cornelisse R., Wijnands R., Homan J., 2007, MNRAS, 380, 1637
Courvoisier T. J.-L. et al., 2003, A&A, 411, L53
Cumming A., Bildsten L., 2001, ApJ, 559, L127
Cumming A., Macbeth J., 2004, ApJ, 603, L37
Cumming A., Macbeth J., in 't Zand J., Page D., 2006, ApJ, 646, 429
Del Monte E., et al., 2008a, Astron. Tel., 1445
Del Monte E. et al., 2008b, A&A, 478, L5
Falanga M., Chenevez J., Cumming A., Kuulkers E., Trap G., Goldwurm A., 2008, A&A, 484, 43
Fender R. P., Kuulkers E., 2001, MNRAS, 324, 923
Fender R. P., Gallo E., Jonker P. G., 2003, MNRAS, 343, L99
Fender R. P., Belloni T. M., Gallo E., 2004, MNRAS, 355, 1105
Feroci M. et al., 2007, Nuclear Instrum. Methods Phys. Res. A, 581, 728
Feroci M. et al., 2010, A&A, 510, A9
Fujimoto M. Y., Hanawa T., Miyaji S., 1981, ApJ, 247, 267
Fujimoto M. Y., Sztajno M., Lewin W. H. G., van Paradijs J., 1987, ApJ, 319, 902
Fushiki I., Lamb D. Q., 1987, ApJ, 323, L55
Galloway D., Cumming A., 2006, ApJ, 652, 559
Galloway D., Psaltis D., Chakrabarty D., Muno M. P., 2003, ApJ, 590, 999
Galloway D., Psaltis D., Muno M. P., Chakrabarty D., 2006, ApJ, 639, 1033
Galloway D. K., Muno M. P., Hartman J. M., Psaltis D., Chakrabarty D., 2008, ApJS, 179, 360 (G08)
Gehrels N. et al., 2004, ApJ, 611, 1005
Grebenev S. A., Molkov S. V., Sunyaev R. A., 2005, Astron. Tel., 467
Gupta S. et al., 2007, ApJ, 662, 1188
Heger A., Cumming A., Galloway D., Woosley S. E., 2007, ApJ, 671, L141
in 't Zand J., Kuulkers E., Verbunt F., Heise J., Cornellise R., 2003, A&A, 411, L487
in 't Zand J. et al., 2004, Nuclear Phys. B, 132, 486
in 't Zand J., Cumming A., van der Sluys M. V., Verbunt F., Pols O. R., 2005, A&A, 441, 675
Jahoda K., Markwardt C. B., Radeva Y., Rots A. H., Stark M. J., Swank J. H., Strohmayer T. E., Zhang W., 2006, ApJS, 163, 401
Keek L., in 't Zand J., 2008, Proceedings of the 7th INTEGRAL PoS(INTEGRAL)032

Keek L., in 't Zand J. J. M., Kuulkers E., Cumming A., Brown E. F., Suzuki M., 2008, A&A, 479, 177
Keek L., Galloway D. K., in 't Zand J. J. M., Heger A., 2010, ApJ, 718, 292
Kennea J. A., Burrows D. N., Markwardt C., Gehrels N., 2005, Astron. Tel., 500
Kuulkers E., 2004, Nuclear Phys. B, 132, 466
Kuulkers E., den Hartog P. R., in 't Zand J. J. M., Verbunt F. W. M., Harris W. E., Cocchi M., 2003, A&A, 399, 663
Kuulkers E. et al., 2002, A&A, 382, 503
Kuulkers E. et al., 2007, A&A, 466, 595
Kuulkers E. et al., 2008, Astron. Tel., 1461
Kuulkers E., in 't Zand J., Lasota J. P., 2009a, A&A, 503, 889
Kuulkers E. et al., 2009b, preprint (arXiv:0909.3391)
Lebrun F. et al., 2003, A&A, 411, L141
Levine A. M., Bradt H., Cui W., 1996, ApJ, 469, L33
Lewin W. H. G., Joss P. C., 1983, in Lewin W. H. G., van den Heuvel E. P. J., eds, Accretion-Driven Stellar X-ray Sources. Cambridge Univ. Press, Cambridge
Lewin W. H. G., van Paradijs J., Taam R., 1993, Space Sci. Rev., 62, 223
Linares M. et al., 2009, Astron. Tel., 1979
Liu Q. Z., van Paradijs J., van den Heuvel E. P. J., 2007, A&A, 469, 807
Lund N. et al., 2003, A&A, 411, L231
Markwardt C. B., Swank J. H., 2005, Astron. Tel., 498
Markwardt C. B., Altamirano D., Swank J. H., in 't Zand J., 2008, Astron. Tel., 1460
Romano P. et al., 2006, A&A, 456, 917
Rothschild R. E. et al., 1998, ApJ, 496, 538
Russell D. M., Maitra D., Dunn R. J. H., Markov S., 2010, MNRAS, 405, 1759
Strohmayer T. E., Bildsten L., 2006, in Lewin W. H. G., van der Klis M., eds, Compact Stellar X-ray Sources. Cambridge Univ. Press, Cambridge, preprint (astro-ph/0301544)
Strohmayer T. E., Brown E. F., 2002, ApJ 566, 1045
Sugimoto D., Ebisuzaki T., Hanawa T., 1984, PASJ, 36, 839
Tavani M. et al., 2008, Nuclear Instrum. Methods Phys. Res. A, 588, 52
Thompson T., Galloway D., Rothschild R., Homer L., 2008, ApJ, 681, 506
Tudose V., Fender R. P., Linares M., Maitra D., van der Klis M., 2009, MNRAS, 400, 2111
Winkler C. et al., 2003, A&A, 411, L1
Yu W., van der Klis M., 2002, ApJ, 567, L67
Zhang S., Chen Y.-P., Wang J.-M., Torres D. F., Li T.-P., 2009, A&A, 502, 231

SUPPORTING INFORMATION

Additional Supporting Information may be found in the online version of this article:

Figure A1. 8-s bin, 17–25 keV light curve of the burst observed by SuperAGILE on 2008 March 26 (MJD 54551.972) prior to the onset of the IGR J17473−2721 outburst.

Figure A2. Chronologically ordered 3–25 keV light curves of the X-ray bursts observed by *INTEGRAL*/JEM-X between MJD 54562 and 54576 (from 1 to 11) and between MJD 54696 and 54711 (from 12 to 14).

Figure A3. Chronologically ordered kT variations of the X-ray bursts observed by *RXTE*/PCA.

Figure A4. Chronologically ordered blackbody radius variations of the X-ray bursts observed by *RXTE*/PCA at a distance $d = 5.5$ kpc.

Figure A5. Plot of the IGR J17473−2721 bursts' exponential decay times ('Edt') as a function of the persistent bolometric flux.

Figure A6. Plot of the *RXTE* bursts' peak fluxes as a function of the burst dual exponential decay times ('Edt').

Table A1. Summary of all burst observations from IGR J17473−2721 in 2008.

Please note: Wiley-Blackwell are not responsible for the content or functionality of any supporting materials supplied by the authors. Any queries (other than missing material) should be directed to the corresponding author for the article.

This paper has been typeset from a TEX/LATEX file prepared by the author.